Synthetic DNA-based nanoswimmers driven by enzyme catalysis

Tania Patiño[1,2]*, Serena Gentile[1], Lorena Baranda[1], Erica Del Grosso[1], Rafael Mestre[3], Samuel Sánchez[4,5], Francesco Ricci[1]*

[1]*Department of Chemical Sciences and Technologies, University of Rome, Tor Vergata, Via della Ricerca Scientifica, 00133 Rome, Italy;*

[2]*Biomedical Engineering Department, Institute for Complex Molecular Systems. Technische Universiteit Eindhoven, Het Kranenveld 14, 5612 AZ Eindhoven The Netherlands.*

[3]*School of Electronics and computer Science (ECS), University of Southampton, University Road, Southampton, SO17 1BJ, United Kingdom.*

[4]*Institute for Bioengineering of Catalonia (IBEC), The Barcelona Institute of Science and Technology (BIST), Baldiri i Reixac 10-12, 08028 Barcelona, Spain;*

[5]*ICREA, Pg. Lluís Companys 23, Barcelona, 08010, Spain.*

*Corresponding Authors, e-mail: t.patino.padial@tue.nl; francesco.ricci@uniroma2.it

ABSTRACT

We report here DNA-based synthetic nanostructures decorated with enzymes (hereafter referred to as DNA enzyme nanoswimmers) that self-propel by converting the enzymatic substrate into the product in solution. The DNA enzyme nanoswimmers are obtained from tubular DNA structures that self-assemble spontaneously by hybridization of DNA tiles. We have functionalized these DNA structures with two different enzymes, urease and catalase, and show that upon addition of the enzymatic substrate (i.e., urea and H_2O_2), they exhibit concentration-dependent motion and different motion dynamics, including enhanced diffusion and ballistic motion. These results pave the way for the development of synthetic enzyme-driven nanoswimmers that can self-propel in fluids and have the potential to provide new insights into biological motion dynamics at the micro-nanoscale.

INTRODUCTION

In the field of DNA nanotechnology, synthetic DNA strands are used to build molecular systems that can exhibit programmable functions of increasing complexity.[1,2] The unique predictability of DNA-DNA interactions allows rationally designed synthetic DNA strands to be used as building blocks for the construction of 2D and 3D nanostructures with defined geometries.[3–7] Synthetic DNA strands can also be site-specifically modified with a wide range of functional components, including optical labels, recognition elements, and proteins,[8] giving otherwise inert DNA-based structures different functionalities. In addition, DNA switches and devices can also be designed to respond to external stimuli such as temperature or pH. [9,10]

The programmability and responsiveness of synthetic DNA described above has been exploited over the past two decades to create DNA-based structures that can perform mechanical work in response to specific

inputs.[11–13] Recently, basic machine elements made of DNA such as hinges, joints, arms, and levers have been demonstrated that can be controlled by DNA-DNA interactions or by environmental stimuli such as pH, ionic strength, temperature, or external fields.[14–17] Recently, for example, Dietz and Simmel described a rotating ratchet motor made entirely of synthetic DNA. The rotor achieves rotational speeds and torques similar to those of other natural molecular machines, such as ATP synthase, and can move in a specific direction by applying a simple external AC field.[18] DNA-based devices and machines can also be developed for molecular transport mechanisms. For example, following the example of kinesin and dynein, which move along microtubules, synthetic DNA walkers have been developed that move along specific 2D and 3D DNA tracks thanks to the programmability of DNA-DNA interactions.[19–21] Despite the above advances in generating motion in DNA-based structures, to our knowledge, no autonomous DNA-based motor has yet been described that can self-propel in fluids and perform net translation (swimming).

In recent years, several synthetic micro- and nanoscale systems have been described that can move in fluids thanks to the application of an external energy source such as magnetic,[22] light,[23] or ultrasonic fields.[24] Other important examples of micro/nanomotors include those driven by chemical reactions between the surface of the motor and a chemical propellant present in solution.[25] A classic example in this regard is the use of catalytic surfaces such as platinum to decompose H_2O_2 in a solution and generate bubbles that propel the micromotor forward.[26] More recently, enzymes have also been used as powerful catalysts to enable self-propulsion of micro- and nanomotors with biocompatible and bioavailable fuels. In this case, micro- and nanoparticles are functionalized with enzymes that catalytically convert a specific substrate into products, creating a chemical gradient around the particles that generates a driving force.[27] These systems offer promising features for biomedical applications, such as the use of biocompatible and bioavailable fuels, chemotactic movement toward or away from chemical gradients, and the absence of external energy sources.[28] Recently, enzyme-driven motors have also been equipped with pH-responsive DNA nanoswitches to create a device that is able to swim and simultaneously sense the pH of its surrounding environment.[29] Despite the above advantages, such enzyme-driven micro/nanomotors also suffer from some limitations. For example, the potential toxicity of their components (metals, silica, and polymers) may limit their application in clinical settings. In addition, it is not always easy to control the geometry and shape of the particles (especially at the nanoscale) in these materials, which could be critical for improving propulsion efficiency. Finally, it is also difficult to achieve efficient surface functionalization with enzymes and to control their distribution and concentration.[30–32]

To overcome the above limitations, we propose here to combine DNA structures with enzyme catalysis to build self-propelled DNA-based nanoswimmers (hereafter referred to as "*DNA-enzyme nanoswimmers*") that would enable easier surface enzyme modification, controlled degradability, biocompatibility, and shape flexibility. As a model system we used a tubular DNA structure and decorated it with a motor enzyme so that the DNA structure is able to move (swim) independently and unhindered in the presence of the enzymatic substrate (Figure 1).

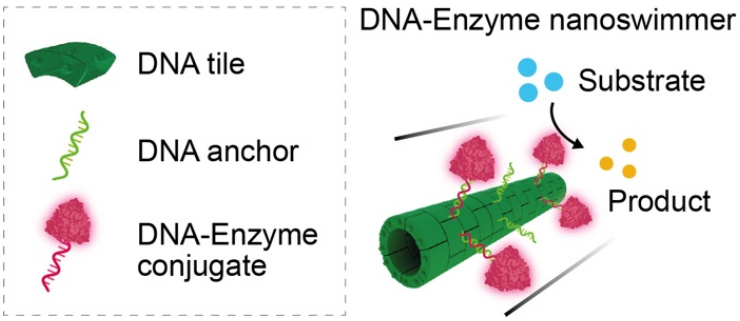

Figure 1. General concept of DNA-enzyme nanoswimmers. *The DNA-enzyme nanoswimmer consists of a structural DNA scaffold with anchor strands that allow decoration with enzymes (by hybridization with DNA-enzyme conjugates). Addition of the enzymatic substrate to such a DNA-enzyme nanoswimmer leads to the formation of the product and self-propulsion.*

RESULTS AND DISCUSSION

The DNA structural scaffold used in this work is a well-characterized hollow tubular micrometer-scale structure formed by the interaction of specifically designed DNA tiles at room temperature. Such DNA tiles are formed by hybridization of five different DNA strands that have 4 sticky ends responsible for self-assembly.[33–35] To directly visualize the assembled tubular structures, we conjugated a Cy3 fluorophore to the 5' end of one of the tile-forming strands. We then engineered another tile-forming strand to have an addressable 30-nucleotides (nt) single-stranded anchor domain that can be used for enzyme functionalization of the structure (Figure S1). The assembled structures can be conveniently imaged by fluorescence microscopy and have an average length and count of 4.9 ± 0.3 μm and 5.2 ± 0.2 x 10^3 count/mm^2, respectively (Figure 2a, right).

For the functionalization with the enzyme, we first selected urease, because this is often used for the development of enzyme-driven micro- and nanoswimmers[27] thanks to the propulsion generated by the conversion of urea ($CO(NH_2)_2$) into ammonium (NH_4^+) and bicarbonate (CO_3^{2-}). More specifically, this movement is thought to be the result of a gradient of ionic products (ionic self-diffusiophoresis) around the swimmer triggered by the enzymatic reaction.[36, ,37] To better visualize the enzyme, we first labeled urease with a Cy5 fluorophore using a Cy5-NHS ester that is reactive toward amine groups in the protein (see Supporting Information for more details). The Cy5-labeled urease was then functionalized with an N3-containing reagent[38] that adds an azide handle to urease by reacting with the amine groups. The resulting azide-Cy5 urease was then conjugated to a dibenzocyclooctyne (DBCO)-modified ssDNA strand using strain-promoted azide-alkyne cycloaddition (SPAAC). The DNA-enzyme conjugate was then purified by anion-exchange chromatography (Figure 2b, right).

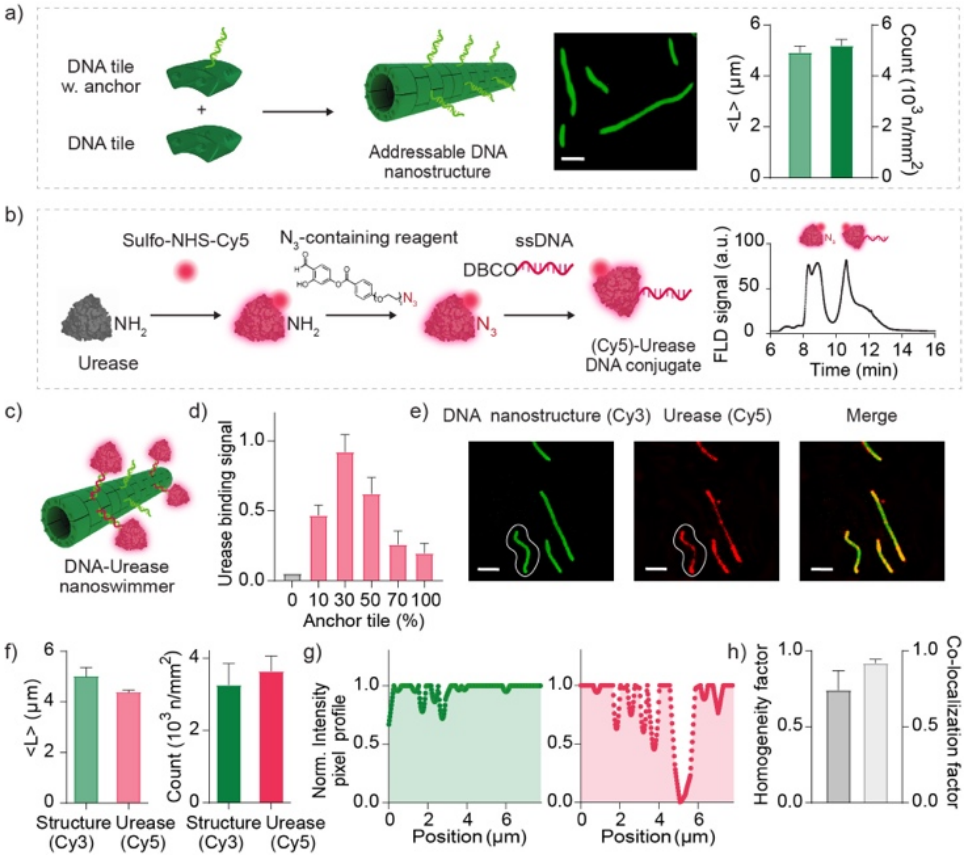

Figure 2. Design and fabrication of DNA-urease structures. *a) Schematic representation of the DNA tile self-assembly process. All DNA tiles are modified with a Cy3 fluorophore. We assembled DNA tiles with a single-stranded anchor strand together with DNA tiles without an anchor strand. An example fluorescence microscopy image showing successful assembly of DNA nanostructures with average length (<L>) and count. b) Reaction scheme of urease conjugation with Cy5 fluorophore and a 30-nt ssDNA. Anion exchange chromatography of the DNA-urease conjugate. c) Schematic representation of DNA-urease nanoswimmer. d) Ratio of urease signal (Cy5) over DNA structure signal (Cy3) for DNA-urease nanoswimmers at different percentages of DNA tiles with anchor strand. e) Representative fluorescence microscopy images obtained with 30% of DNA tiles with anchor strand. f) Average length and count obtained by using both urease (Cy5) and DNA structure (Cy3) signals. g) Pixel intenstity of urease (Cy5) and DNA structure (Cy3) signals along the length of a DNA structure. h) Homogeneity factor and proportion of Cy5 pixels (urease) colocalizing with Cy3 pixels (DNA structure). Scale bar: 3.0 μm. Experiments were performed in 12.5 mM $MgCl_2$ solution, at T = 25 °C with 50 nM of DNA nanostructures. Error bars represent standard deviation based on triplicate measurements.*

To find the best conditions for enzyme functionalization, we assembled DNA structures with different percentage distribution of the anchor strand by using different proportions of tiles with and without anchor strand during self-assembly. The efficiency of the self-assembly process was not affected by the presence of the anchor strand, as the size and number of nanostructures formed did not show significant differences in the absence and presence of different proportions of anchor strands (Figures S2, S3). To all assembled structures, we then added the DNA strand conjugated with urease at a fixed excess concentration (i.e., 200 nM) and quantified the mean fluorescence intensity of Cy5 urease on the surface of the DNA structures (Cy3). The binding of the enzyme to the

structure increases with the percentage of tiles with the anchor strand until it levels off at 50%. By further increasing the relative proportion of anchor strands in the structure, less enzyme decoration is observed, likely due to enzyme aggregation effects (Figures 2c-d, S4). For future experiments, we then selected DNA structures containing 30% of the tiles with the anchor strand (Figure 2e). Under these conditions, we find a homogeneous distribution of urease across the DNA structures. For example, the values for the average length (Cy3-DNA structure: 5.0 ± 0.3; Cy5-urease: 4.4 ± 0.1 μm) and count (Cy3-DNA structure: 3.3 ± 0.6; Cy5-urease: 3.6 ± 0.4 x 10^3 count/mm^2) obtained by measuring either the Cy3 (DNA tiles) or Cy5 (enzyme) signals are comparable (Figure 2f). The homogenous enzyme distribution is also confirmed by analysing the pixel intensity of DNA tiles and urease along the entire length of a single DNA structure (Figure 2g). From these analyses we derived a homogeneity factor (defined here as the average ratio of urease (Cy5) signal to DNA structure signal (Cy3) along the length of the DNA structure) of 0.7 ± 0.1. Finally, to better quantify the distribution of urease on the DNA structure, we calculated a co-localization factor that we used to estimate the overlap of the urease signal (Cy5) with the DNA structure signal (Cy3). A value of this factor around 1 would indicate a high co-localization of the enzyme with the DNA structure, whereas no overlap would result in a value around 0. In our case, a co-localization factor of 0.9 ± 0.1 suggests that the enzyme is highly co-localised with the DNA tiles (Figure 2h).

Next, we investigated the movement capabilities of urease-functionalized DNA structures. To induce active movement, we exposed the structures to different concentrations of urea (from 10 to 300 mM) (Figure 3a). We recorded videos of 30 seconds duration at a rate of 20 frames per second (see Supporting Videos 1 and 2). To track the trajectories of the DNA-enzyme nanoswimmers, we developed the Nano-Micromotor Tracking Tool (NMTT) v 1.0.0, a Python-based script that uses computer vision techniques to track the position of one or more particles in time[39] (see details in Supporting Methods), which allowed us to calculate the mean square displacement (MSD), diffusion coefficient, and speed of the motors (see Supporting Information). Snapshots of nanoswimmer motion trajectories 30 seconds after the addition of urea show significantly longer trajectories for nanoswimmers exposed to 100 mM and 300 mM urea compared to those obtained in the absence of urea. Representative trajectories of different motion experiments under these conditions (0, 100, and 300 mM urea) are also shown in Figure 3c. From these trajectories, the MSD and associated motion parameters can be extracted using the Python-based Nano-Micromotor Analysis Tool (NMAT) v 1.0.0[40] (Figure 3d, left). We observed a clear correlation between the amount of fuel and the MSD of DNA enzyme nanoswimmers, in a concentration-dependent manner. With increasing urea concentration, the MSD shows a deviation from linear diffusion to a non-linear MSD characteristic of self-propelled motion. [41,42] This is particularly visible in the case of 300 mM urea. Given their anisotropic shape and the homogeneous distribution of enzymes, one would not expect these nanotubes to exhibit ballistic motion, but only some degree of anomalous superdiffusion defined by an MSD scaling parameter $1< \alpha < 2$, as appears to be the case (Figure S5).[43] In the absence of a clear theory of active Brownian motion that would allow us to clearly characterize this case, we decided to investigate both the effective diffusion coefficient (Figure 3e) and the effective speed (Figure 3f) under an active Brownian motion regime with a ballistic component. We observed a concentration-dependent increase for both parameters, with a concentration of 300 mM leading to a significant increase in both the effective diffusion coefficient and speed.

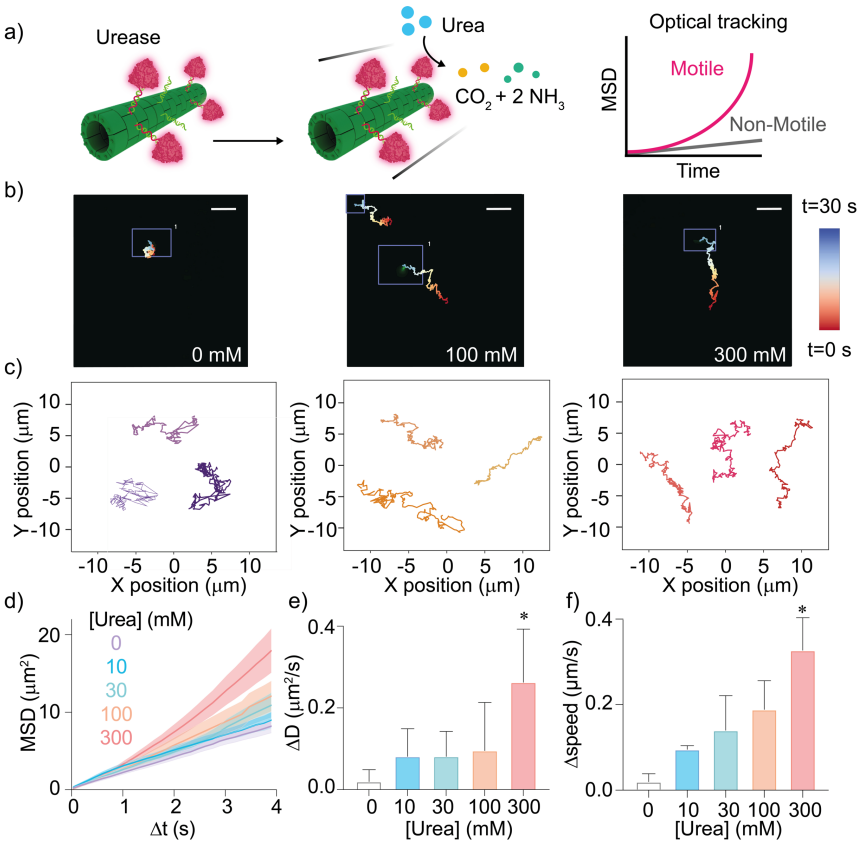

Figure 3. DNA-based nanoswimmers propelled by urease. *a) Schematic representation of the propulsion mechanism and motion analysis. b) Snapshots of nanoswimmers exposed to different fuel concentrations at t=30s. Scale bar: 10 μm. c) Representative trajectories of nanoswimmers at 0 (left), 100 (middle) and 300 (right) mM urea. d,e, f) MSDs, effective diffusion coefficient and effective speed of the nanoswimmers at increasing fuel concentrations. Error bars represent standard deviation based on an average of N=20 videos recorded.*

To exclude any effect of the fuel concentration on the diffusivity of the swimmers, we exposed the DNA structures without urease on their surface to concentrations of 0, 100 and 300 mM urea. Non-functionalized DNA nanostructures exposed to 0 and 100 mM urea showed a linear MSD, indicating purely diffusive motion, without significant differences (measured effective diffusion coefficient 0.7 ± 0.3 $\mu m^2/s$ and 0.6 ± 0.2 $\mu m^2/s$, respectively) (Figure S6). In the case of DNA nanostructures, without urease, exposed to 300 mM urea, we could not track their trajectories because the DNA nanostructures disassembled during video recording (see Supporting Video 3). We attribute this effect to the fact that urea at high concentrations is a DNA denaturing agent, causing the destabilization of the double DNA helix structure. Interestingly, we did not observe this effect in urease-functionalized nanoswimmers. We explain this difference by the fact that urease continuously converts urea, which leads to a decrease in the local urea concentration and thus preserves the stability of the DNA nanostructure.

Next, we explored the potential versatility of our DNA enzyme nanoswimmers by using another enzyme as a source of self-propulsion (Figure 4). For this purpose, we chose catalase, the most commonly used enzymatic drive for self-propelled micro- and nanomotors.[44,45] Catalase is capable of converting hydrogen peroxide (H_2O_2) into water and oxygen (O_2), which can lead to self-propulsion by i) the generation of bubbles or ii) a diffusiophoretic

motion mechanism. We conjugated catalase to ssDNA strands using a reaction similar to that used to prepare urease-DNA conjugates (see the experimental section in the supporting information and Figure S6). We then functionalized the DNA nanostructures using 30% of the tiles with anchor strand (as in the case of DNA urease nanoswimmers) (Figure 4a). We detected the presence of catalase (Cy3) on the surface of the DNA nanostructures (Cy5) using fluorescence microscopy images (Figure 4b). Comparable values for average length (Cy5 DNA structure: 2.8 ± 0.3; Cy3 catalase: 2.3 ± 0.2 μm) and count (Cy5 DNA structure: 4.4 ± 0.2; Cy3 catalase: 4.4 ± 0.4 x 10^4 counts/mm^2) were obtained, demonstrating a homogeneous distribution of catalase in the DNA structure (Figure 4c). Such a homogeneous distribution was also confirmed by analysis of the signals from the enzyme and DNA tiles along the DNA structure (homogeneity factor: 0.8 ± 0.1) (Figure 4d-e). Finally, we also found a high degree of co-localization of catalase with the DNA structure in this case (co-localization factor = 0.9 ± 0.1) (Figure 4e). Next, we examined the motility of the catalase-DNA swimmers when exposed to 1.5% H_2O_2 (see Supporting Videos 4 and 5). The nanoswimmers showed longer trajectories (Figure 4f), higher MSD (Figure 4g), higher effective diffusion coefficient (Figure 4h), and speed (Figure 4i). Similar to the case of urease nanoswimmers, we found a value of the MSD exponent of $1< \alpha < 2$ (see Supporting Figure 8) for the nanoswimmers in presence of fuel. For this reason, we decided to analyse both effective diffusion coefficient and effective speed. The average effective diffusion coefficient for catalase DNA swimmers without fuel was 0.6 ± 0.3 $\mu m^2/s$ (mean ± SD), whereas the effective diffusion coefficient increased to 0.9 ± 0.6 $\mu m^2/s$ in the presence of propellant. As for the effective speed, a mean value of 0.5 ± 0.2 μm/s was observed for the nanoswimmers exposed under control conditions, which increased to 0.9 ± 0.4 μm/s. Both the increase in effective diffusion coefficient and effective speed were statistically significant ($P < 0.05$).

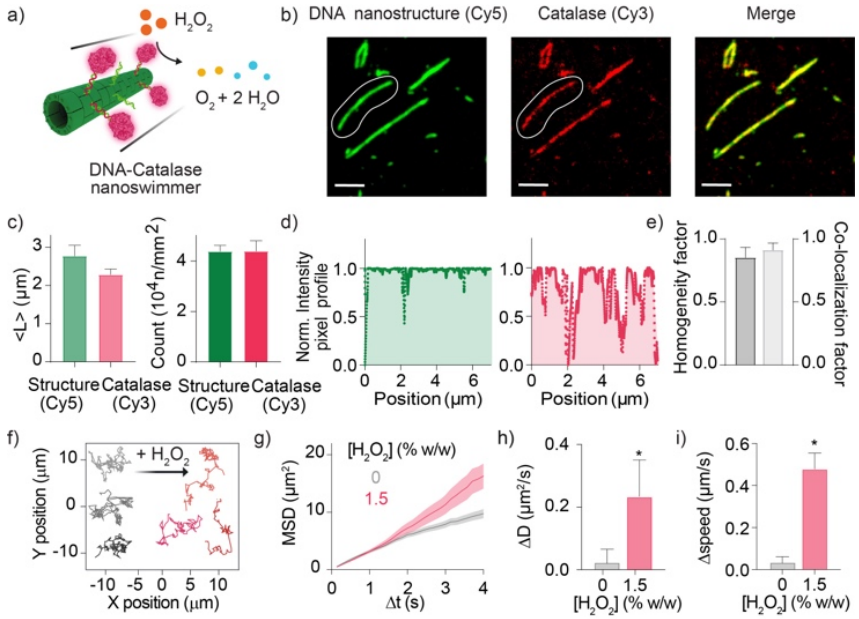

Figure 4. Motility of catalase-driven DNA-based nanoswimmers. *a) Schematic representation of the propulsion mechanism. b) Representative fluorescence microscopy images of DNA nanostructures with 30% of DNA tiles with anchor strand(Cy5) functionalized with catalase (Cy3). Scale bar: 3.0 μm. (c) Average length and number determined from DNA structure (Cy5) and catalase (Cy3) signals. Error bars represent standard deviation based on triplicate measurements. d) Pixel*

intensity of DNA structure (Cy5) and catalase (Cy3) signals along the length of a DNA structure. e) Homogeneity factor and fraction of Cy3 (catalase) pixels colocalizing with Cy5 (DNA structure) pixels. f) Representative trajectories of nanoswimmers exposed to different fuel concentrations (0 and 1.5 (% w/w) H_2O_2) at t=30s. g,h, i) MSDs, effective diffusion coefficient and effective speed of nanoswimmers at 0 and 1.5 % w/w H_2O_2 concentration. Error bars represent the standard deviation based on an average of N=20 videos recorded. Experiments were performed in 12.5 mM $MgCl_2$ solution at T = 25 °C with 50 nM DNA nanostructures and 200 nM DNA catalase conjugate.

CONCLUSION

Taken together, our results show that synthetic DNA has great potential as a building block for creating artificial nanoscale molecular motors that can self-propel in fluids. In addition, thanks to the use of enzymes, biologically available and biocompatible fuels can be used as a source of self-propulsion. We believe that the results reported here will pave the way to more sophisticated designs of DNA-based enzyme-powered motors, where synthetic DNA can lead to the discovery of new structural designs and allow programmable control of the decoration of enzymes and other biomolecules on their surfaces. The above properties, together with the sequence specificity of the DNA-DNA interactions, may enable the construction of enzyme-driven DNA motors that can respond to different substrates in the same solution and perform different motion dynamics in a fuel-dependent manner, paving the way for new approaches to understanding nanoscale motion and enabling better control over the design and functionality of nano/micro-swimmers.

ACKNOWLEDGMENT

This work was supported by European Union's Horizon 2020 research and innovation program, under the Marie Skłodowska-Curie Individual Fellowship (843998 to TP and 896962 to EDG), the European Research Council, ERC (819160 to FR and 866348 to SS), by the Irène Curie Fellowship (TP), Associazione Italiana per la Ricerca sul Cancro, AIRC (project n. 21965) (FR).

REFERENCES

(1) Seeman, N. C.; Sleiman, H. F. DNA Nanotechnology. *Nat Rev Mater* **2017**, 3, 17068.

(2) Keller, A.; Linko, V. Challenges and Perspectives of DNA Nanostructures in Biomedicine. *Angew Chem Int Ed* **2020**, 59, 15818–15833.

(3) Chen, J.; Seeman, N. C. Synthesis from DNA of a Molecule with the Connectivity of a Cube. *Nature* **1991**, 350, 631–633.

(4) Winfree, E.; Liu, F.; Wenzler, L. A.; Seeman, N. C. Design and Self-Assembly of Two-Dimensional DNA Crystals. *Nature* **1998**, 394, 539–544.

(5) Rothemund, P. W. K. Folding DNA to Create Nanoscale Shapes and Patterns. *Nature* **2006**, 440, 297–302.

(6) Wei, B.; Dai, M.; Yin, P. Complex Shapes Self-Assembled from Single-Stranded DNA Tiles. *Nature* **2012**, 485, 623–626.

(7) Veneziano, R.; Ratanalert, S.; Zhang, K.; Zhang, F.; Yan, H.; Chiu, W.; Bathe, M. Designer Nanoscale DNA Assemblies Programmed from the Top Down. *Science* **2016**, 352, 1534–1534.

(8) Ranallo, S.; Porchetta, A.; Ricci, F. DNA-Based Scaffolds for Sensing Applications. *Anal Chem* **2019**, 91, 44–59.

(9) Idili, A.; Vallée-Bélisle, A.; Ricci, F. Programmable PH-Triggered DNA Nanoswitches. *J Am Chem Soc* **2014**, 136, 5836–5839.

(10) Liu, J.; Li, W.; Li, R.; Yin, X.; He, S.; Hu, J.; Ruan, S. Programmable DNA Framework Sensors for In Situ Cell-Surface PH Analysis. *Anal Chem* **2021**, 93, 12170–12174.

(11) Dey, S.; Fan, C.; Gothelf, K. V.; Li, J.; Lin, C.; Liu, L.; Liu, N.; Nijenhuis, M. A. D.; Saccà, B.; Simmel, F. C.; Yan, H.; Zhan, P. DNA Origami. *Nat Rev Methods Primers* **2021**, 1, 13.

(12) Wang, J.; Li, Z.; Willner, I. Dynamic Reconfigurable DNA Nanostructures, Networks and Materials. *Angew Chem Int Ed* **2023**, 62, e202215332.

(13) Knappe, G. A.; Wamhoff, E.-C.; Bathe, M. Functionalizing DNA Origami to Investigate and Interact with Biological Systems. *Nat Rev Mater* **2022**, 8 , 123–138.

(14) List, J.; Falgenhauer, E.; Kopperger, E.; Pardatscher, G.; Simmel, F. C. Long-Range Movement of Large Mechanically Interlocked DNA Nanostructures. *Nat Commun* **2016**, 7, 12414.

(15) Ketterer, P.; Willner, E. M.; Dietz, H. Nanoscale Rotary Apparatus Formed from Tight-Fitting 3D DNA Components. Sci Adv **2016**, 2, e1501209.

(16) Ramezani, H.; Dietz, H. Building Machines with DNA Molecules. Nat Rev Genet **2020**, 21, 5–26.

(17) Marras, A. E.; Zhou, L.; Su, H.-J.; Castro, C. E. Programmable Motion of DNA Origami Mechanisms. *Proc Nat Acad Sci U.S.A*. **2015**, 112, 713–718.

(18) Pumm, A.-K.; Engelen, W.; Kopperger, E.; Isensee, J.; Vogt, M.; Kozina, V.; Kube, M.; Honemann, M. N.; Bertosin, E.; Langecker, M.; Golestanian, R.; Simmel, F. C.; Dietz, H. A DNA Origami Rotary Ratchet Motor. *Nature* **2022**, 607, 492–498.

(19) Wickham, S. F. J.; Bath, J.; Katsuda, Y.; Endo, M.; Hidaka, K.; Sugiyama, H.; Turberfield, A. J. A DNA-Based Molecular Motor That Can Navigate a Network of Tracks. *Nat Nanotechnol.* **2012**, 7, 169–173.

(20) Yehl, K.; Mugler, A.; Vivek, S.; Liu, Y.; Zhang, Y.; Fan, M.; Weeks, E. R.; Salaita, K. High-Speed DNA-Based Rolling Motors Powered by RNase H. *Nat Nanotechnol* **2016**, 11, 184–190.

(21) Omabegho, T.; Sha, R.; Seeman, N. C. A Bipedal DNA Brownian Motor with Coordinated Legs. *Science* **2009**, 324, 67–71.

(22) Zhou, H.; Mayorga-Martinez, C. C.; Pané, S.; Zhang, L.; Pumera, M. Magnetically Driven Micro and Nanorobots. *Chem Rev* **2021**, 121, 4999–5041.

(23) Yuan, K.; Bujalance-Fernández, J.; Jurado-Sánchez, B.; Escarpa, A. Light-Driven Nanomotors and Micromotors: Envisioning New Analytical Possibilities for Bio-Sensing. *Microchimica Acta* **2020,** 187, 581.

(24) Hansen-Bruhn, M.; de Ávila, B. E. F.; Beltrán-Gastélum, M.; Zhao, J.; Ramírez-Herrera, D. E.; Angsantikul, P.; Vesterager Gothelf, K.; Zhang, L.; Wang, J. Active Intracellular Delivery of a Cas9/SgRNA Complex Using Ultrasound-Propelled Nanomotors. *Angew Chem Int Ed* **2018**, 57, 2657–2661.

(25) Sánchez, S.; Soler, L. L.; Katuri, J.; Sanchez, S.; Soler, L. L.; Katuri, J.; Sánchez, S.; Soler, L. L.; Katuri, J. Chemically Powered Micro- and Nanomotors. *Angew Chem Int Ed* **2015**, 54, 1414–1444.

(26) Zhang, Y.; Hess, H. Chemically-Powered Swimming and Diffusion in the Microscopic World. *Nat Rev Chem* **2021**, 5, 500–510.

(27) Arqué, X.; Patiño, T.; Sánchez, S. Enzyme-Powered Micro- and Nano-Motors: Key Parameters for an Application-Oriented Design. *Chem Sci* **2022**, 13, 9128–9146.

(28) Somasundar, A.; Ghosh, S.; Mohajerani, F.; Massenburg, L. N.; Yang, T.; Cremer, P. S.; Velegol, D.; Sen, A. Positive and Negative Chemotaxis of Enzyme-Coated Liposome Motors. *Nat Nanotechnol* **2019**, 14, 1129–1134 .

(29) Patino, T.; Porchetta, A.; Jannasch, A.; Lladó, A.; Stumpp, T.; Schäffer, E.; Ricci, F.; Sánchez, S. Self-Sensing Enzyme-Powered Micromotors Equipped with PH-Responsive DNA Nanoswitches. *Nano Lett **2019***, 19, 3440–3447.

(30) Patiño, T.; Feiner-Gracia, N.; Arqué, X.; Miguel-López, A.; Jannasch, A.; Stumpp, T.; Schäffer, E.; Albertazzi, L.; Sánchez, S. Influence of Enzyme Quantity and Distribution on the Self-Propulsion of Non-Janus Urease-Powered Micromotors. *J Am Chem Soc* **2018**, 140, 7896–7903.

(31) Song, S.; Mason, A. F.; Post, R. A. J.; De Corato, M.; Mestre, R.; Yewdall, N. A.; Cao, S.; van der Hofstad, R. W.; Sanchez, S.; Abdelmohsen, L. K. E. A.; van Hest, J. C. M. Engineering Transient Dynamics of Artificial Cells by Stochastic Distribution of Enzymes. *Nat Commun* **2021**, 12, 6897.

(32) Yang, Y.; Arqué, X.; Patiño, T.; Guillerm, V.; Blersch, P.R.; Pérez-Carvajal, J.; Imaz, I.; Maspoch, D.; Sánchez, S. Enzyme-Powered Porous Micromotors Built from a Hierarchical Micro- and Mesoporous UiO-Type Metal–Organic Framework. *J Am Chem Soc* **2020**, 142, 20962–20967.

(32) Ranallo, S.; Sorrentino, D.; Ricci, F. Orthogonal Regulation of DNA Nanostructure Self-Assembly and Disassembly Using Antibodies. *Nat Commun* **2019**, 10, 5509.

(32) Gentile, S.; Del Grosso, E.; Prins, L. J.; Ricci, F. Reorganization of Self-assembled DNA-based Polymers Using Orthogonally Addressable Building Blocks. *Angew Chem Int Ed* **2021**, 60, 12911.

(33) Gentile, S.; Del Grosso, E.; Pungchai, P. E.; Franco, E.; Prins, L. J.; Ricci, F. Spontaneous Reorganization of DNA-Based Polymers in Higher Ordered Structures Fueled by RNA. *J Am Chem Soc* **2021**, 143, 20296–20301.

(34) Rothemund, P. W. K.; Ekani-Nkodo, A.; Papadakis, N.; Kumar, A.; Fygenson, D. K.; Winfree, E. Design and Characterization of Programmable DNA Nanotubes. *J Am Chem Soc* **2004**, 126, 16344–16352.

(35) Green, L. N.; Subramanian, H. K. K.; Mardanlou, V.; Kim, J.; Hariadi, R. F.; Franco, E. Autonomous Dynamic Control of DNA Nanostructure Self-Assembly. *Nat Chem* **2019**, 11, 510–520.

(36) Arqué, X.; Andrés, X.; Mestre, R.; Ciraulo, B.; Ortega Arroyo, J.; Quidant, R.; Patiño, T.; Sánchez, S. Ionic Species Affect the Self-Propulsion of Urease-Powered Micromotors. *Research* **2020**, 2020, 1–14.

(37) De Corato, M.; Arqué, X.; Patiño, T.; Arroyo, M.; Sánchez, S.; Pagonabarraga, I. Self-Propulsion of Active Colloids via Ion Release: Theory and Experiments. *Phys Rev Lett* **2020**, 124, 108001.

(38) Baranda Pellejero, L.; Nijenhuis, M. A. D.; Ricci, F.; Gothelf, K. V. Protein-Templated Reactions Using DNA-Antibody Conjugates. *Small* **2023**, 19, 202200971.

(39) Mestre, R. Rafamestre/NMTT-Nanomicromotor-Tracking-Tool: NMTT v1.0.0. 2022. https://doi.org/10.5281/ZENODO.5905482.

(40) Mestre, R. Rafamestre/NMAT-Nanomicromotor-Analysis-Tool: NMAT v1.0.0. 2022. https://doi.org/10.5281/ZENODO.5905486.

(41) Dunderdale, G.; Ebbens, S.; Fairclough, P.; Howse, J. Importance of Particle Tracking and Calculating the Mean-Squared Displacement in Distinguishing Nanopropulsion from Other Processes. *Langmuir* **2012**, 28, 10997–11006.

(42) Howse, J. R.; Jones, R. A. L.; Ryan, A. J.; Gough, T.; Vafabakhsh, R.; Golestanian, R. Self-Motile Colloidal Particles : From Directed Propulsion to Random Walk. *Phys Rev Lett* **2007**, 99, 8–11.

(43) Mestre, R.; Palacios, L. S.; Miguel-López, A.; Arqué, X.; Pagonabarraga, I.; Sánchez, S. Extraction of the Propulsive Speed of Catalytic Nano- and Micro-Motors under Different Motion Dynamics. arXiv **2020**, arXiv:2007.15316.

(44) Sanchez, S.; Solovev, A. A.; Mei, Y.; Schmidt, O. G. Dynamics of Biocatalytic Microengines Mediated by Variable Friction Control. *J Am Chem Soc* **2010**, 132, 13144–13145.

(45) Ma, X.; Hortelao, A. C.; Miguel-López, A.; Sánchez, S. Bubble-Free Propulsion of Ultrasmall Tubular Nanojets Powered by Biocatalytic Reactions. *J Am Chem Soc* **2016**, 138, 13782–13785.